Pedram Loghmannia and Majid Manteghi

Broadband Parametric Impedance Matching for Small Antennas Using the Bode-Fano Limit

Improving on Chu's limit for loaded small antennas.

xxxxx

In this work, a parametric up-converter amplifier is introduced as a wideband impedance-matching network. Chu's limit restricts the minimum Q-factor of unloaded small antennas. However, the practical bandwidth (BW) of small antennas is defined by their loaded Q-factor. By connecting a small antenna to an amplifier with a real input impedance that is several times greater than the radiation resistance of the antenna, we propose increasing the return loss, which leads to a reduction in the loaded Q-factor and an increase in the BW. In addition, a parametric amplifier is used because, in comparison with transistor amplifiers, it offers low-noise characteristics. The gain of the low-noise parametric amplifier compensates for the loss due to the imposed mismatch. Our simulation result shows BW improvements up to 32 times can be accomplished by trading 2 dB of noise figure (NF), compared to the 15 dB suggested by Chu's limit for a lossy antenna.

INTRODUCTION

Electrically small antennas (ESAs) are an inseparable part of a wide range of very-high-frequency and ultrahigh-frequency transceivers, implanted devices, the Internet of Things, and so on. Demands for higher data rates encourage the use of broadband antennas by radio engineers. However, alongside Wheeler and Chu's findings [1], [2], the Bode-Fano bound [3] shows that the realized gain of ESAs needs to be traded for broader BW. Essentially, Chu's limit ties the Q-factor of a lossless antenna to the inverse of its electric size to the power of three. This relationship shows how fast the realized gain-BW product is decreased by miniaturization.

Chu's limit was established based on a single-mode and linear time-invariant (LTI) antenna; thus, efforts have been made since the 1950s to crack the limit using multimode and/or non-LTI techniques for ESAs [4]–[6]. On one hand, almost all non-LTI techniques, especially for high-power applications, have been implemented for transmit antennas [4]. On the other hand, wireless-network engineers have had an understanding that part of the loss associated with mismatch and poor radiation efficiency of ESAs could be compensated with low-noise amplification on the receiving side [e.g., short-wave and long-wave radio receivers (Rxs)]. Nevertheless, utilizing an active component deteriorates the overall NF since the amplification happens after the antenna stage. The literature has also suggested many methods to increase an ESA's BW using active

Digital Object Identifier 10.1109/MAP.2021.3089997
Date of current version: 12 July 2021

matching or non-Foster matching techniques [7]–[11]. In [12], it was shown that the total noise voltage generated in the Linvill negative-impedance converter (NIC) is proportional to the magnitude of the NIC input impedance. In other words, the larger reactance that the NIC (non-Foster technique) cancels, the higher the deterioration of the noise performance of the non-Foster technique.

Due to their applications in the magnetless nonreciprocal devices [13]–[15] and low-noise active antennas [16], [17], parametric devices as nonlinear and/or time-variant components have recently regained the attention of researchers. Although parametric amplifiers are low-noise components compared to the transistor counterparts due to their reactive nature, to the best of our knowledge, they have not been used in any ESA-matching circuit on the receiving side. This article introduces an active matching methodology that dramatically increases an ESA's instantaneous BW on the receiving side while it not increasing the NF at the same rate.

As presented in Figure 1(a), the most traditional way of using magnetic (i.e., highly inductive) ESA is connecting it to a matched load leading to an extremely narrow BW. Figure 1(b) displays one way to increase the BW: by adding loss to the antenna, which results in $(3 \times N)$-dB-added noise for 2^N-times BW improvement. Another way, illustrated in Figure 1(c), is removing the tuning capacitor and connecting the antenna directly to a pure real impedance, leading to poor noise performance due to a huge mismatch.

We believe, by inspiration of the Bode-Fano limit, that tuning the antenna at the desired frequency and connecting it to a pure impedance several times greater than the real part of the antenna-input impedance [see Figure 1(d)] gives the best tradeoff between BW improvement and added noise as explained in the "Background of ESAs and Their BW Improvement Using the Bode-Fano Bound" section of this article. To the authors' best knowledge, the circuit displayed in Figure 1(d) has never been used in the context of widening the BW of the small antennas. Because the antenna is working on the receiving side, in all of the four circuits presented in Figure 1, R_L represents the input impedance of an amplifier.

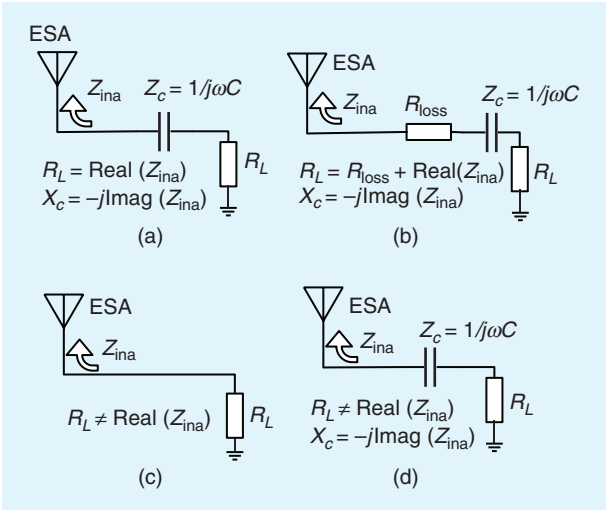

FIGURE 1. The different ways of loading a magnetic ESA: (a) matched case, (b) adding loss, (c) direct connection, and (d) tuned case using the Bode-Fano theorem (our method).

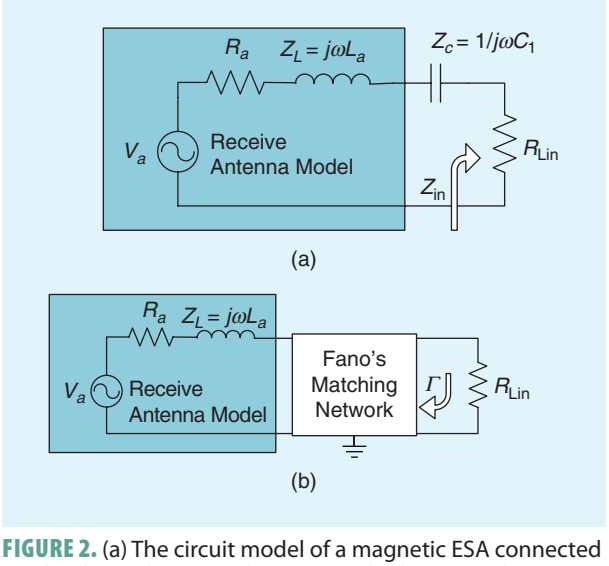

FIGURE 2. (a) The circuit model of a magnetic ESA connected to a load, R_{Lin}. (b) Fano's theorem applied to a simple *RL* circuit.

BACKGROUND OF ESAs AND THEIR BW IMPROVEMENT USING THE BODE-FANO BOUND

In 1948, Chu considered a small magnetic antenna enclosed in a sphere of radius a [1] and showed the equivalent circuit of the small magnetic antenna is a series *RC* (i.e., a resistor in series with a capacitor) in parallel with an inductance *L*. However, the resulting poles in the complex frequency plane are located far above the frequency range so that the antenna is still considered small. Furthermore, an ESA has recently been shown to be similar to a lossy inductor (magnetic antenna, e.g., small-loop antenna) or lossy capacitor (electric antenna, e.g., a short-dipole antenna) [4]. The simplified models of the electrically small magnetic and electric antennas are series *RL* and series *RC*, respectively. An ESA's quality factor was demonstrated to be

$$Q_a = \frac{1}{(ka)^3}, \tag{1}$$

where k is the free-space wavenumber.

Chu calculated the antenna-unloaded Q-factor. However, we need to load the antenna with an external circuit [Rx or transmitter (Tx)] in practical applications. Thus, it is necessary to define the BW of the antenna based on the loaded Q-factor. That is why Chu referred to Fano's paper [3] for the relationship between his Q-factor and the antenna BW.

Figure 2(a) shows the equivalent circuit (series *RL*) of a receiving magnetic ESA connected to a load, R_{Lin}, as the Rx load. R_a, L_a, and V_a represent antenna-radiation resistance (in addition to the antenna loss), inductance, and open-circuit

voltage, respectively. Moreover, C_1 represents the tuning capacitor in addition to the parasitic capacitor associated with the antenna structure.

Based on Figure 2(a), the Q-factor of the loaded antenna is

$$Q_L = \frac{2\pi f L_a}{R_a + R_{Lin}}, \tag{2}$$

where f is the center frequency of the tuned antenna. However, the Q-factor for the unloaded antenna model is obtained by setting $R_{Lin} = 0$ as

$$Q_a = \frac{2\pi f L_a}{R_a}. \tag{3}$$

As seen, it is possible to decrease the loaded Q-factor by increasing R_{Lin}, leading to a broader BW. However, simple analysis shows that setting R_{Lin} to any value other than R_a reduces the power delivered to R_{Lin} due to the mismatch at the resonant frequency.

Fano rigorously studied the previous concept and mathematically formulated it [3]. His work has resulted in some integral equations defining a tradeoff between matching BW and realized gain (efficiency associated with return loss).

Figure 2(b) displays a simple series RL circuit as a complex source impedance ($R_a + j\omega L_a$). Fano's simplified integral to match this RL circuit to a purely resistive load R_{Lin} is

$$\int_0^\infty \ln\frac{1}{|\Gamma(f)|}df \le \frac{R_a}{2L_a}, \tag{4}$$

where Γ is the reflection coefficient between the matching circuit and the load. Fano showed that the right side of (4) places an upper limit on the $\ln(1/|\Gamma|)$ region over the entire frequency band for the prescribed L_a and R_a. A small value of R_a/L_a reduces the upper limit, resulting in a reduction of the region under integration (higher Q_a and lower realized-gain-BW product).

Considering a constant value for $\ln(1/|\Gamma|) = \max[\ln(1/|\Gamma|)]$ in the desired frequency range, and making it zero at other frequencies [3] leads to the efficient use of the area under the integration and to the maximization of the BW:

$$\Delta f_{\max} = \frac{0.5}{(L_a/R_a)\max[\ln(1/|\Gamma|)]}. \tag{5}$$

Considering L_a and R_a in series as the circuit model of a magnetic ESA, we can use (3) and (5) to link the Bode-Fano to Chu's Q-factor as

$$\frac{\Delta f_{\max}}{f} = \frac{\pi}{Q_a \times \max[\ln(1/|\Gamma|)]}. \tag{6}$$

This equation shows that the maximum BW is proportional to the inverse of Chu's unloaded Q-factor times $\ln 1/|\Gamma|$. Because one can amplify the received signal utilizing an amplifier, the only limitation to increasing the BW of a high-Q receiving antenna is the signal-to-noise ratio (S_r/N_r) of the received signal.

Based on Poynting's theorem, the available power density at the antenna aperture is $W^i = |\boldsymbol{E}^i|^2/(2\eta)$, and the open-circuit voltage at the antenna port is $V_a = \mathbf{E}^i \cdot \mathbf{l}_{\text{eff}}$ which peaks for matched polarization at $V_a^{\max} = |E^i l_{\text{eff}}|$. Thus, the maximum power delivered to R_{Lin} is

$$\max(P_{\text{del}}) = \frac{\eta}{2R_a} W^i l_{\text{eff}}^2 (1 - |\Gamma|^2) = \frac{1}{4R_a} V_a^2 (1 - |\Gamma|^2), \tag{7}$$

where Γ is the return loss of the Fano's matching network connected to the antenna seen from R_{Lin} [Figure 2(b)]. The maximum power delivered to R_{Lin} is one half of the power generated by V_a (for $\Gamma = 0$), and the antenna backscatters (reradiates) at least one half of the power (the dissipated power in R_a). A higher mismatch (equivalent to wider BW) can increase the backscattered power from the aperture of the receiving antenna from 50% to 100% (for $|\Gamma| = 1$).

To show the gain-BW limitation, we have synthesized a fourth-order matching circuit based on the Bode-Fano method [3] for $\max(\ln[1/|\Gamma|]) = 0.348$ and 0.052, corresponding to 3-dB and 10-dB reduction in the gain. The results of the Advanced Design System (ADS) simulations are provided in Figure 3 and are compared to both the ideal case (6) and the simple-conjugate matched case corresponding to Figure 2(a) with $R_a = R_{Lin}$.

By reducing the realized gain (higher backscattering by implementing mismatch), one can dramatically increase the BW of a high-Q antenna. Now, let us take R_{Lin} as the input impedance of an active circuit like an amplifier, as presented in Figure 4. We can set the amplifier gain to 3 dB or 10 dB, respectively, to account for 3-dB or 10-dB losses. In the absence of noise, the antenna BW is improved, and its gain is remedied by an amplifier while still constrained by the Fano's bound (it did not go beyond the Fano's bound, which contradicts the statements in [18]).

In reality, utilizing active components degrades the receiving-system NF. The NF of the front end of the Rx presented in

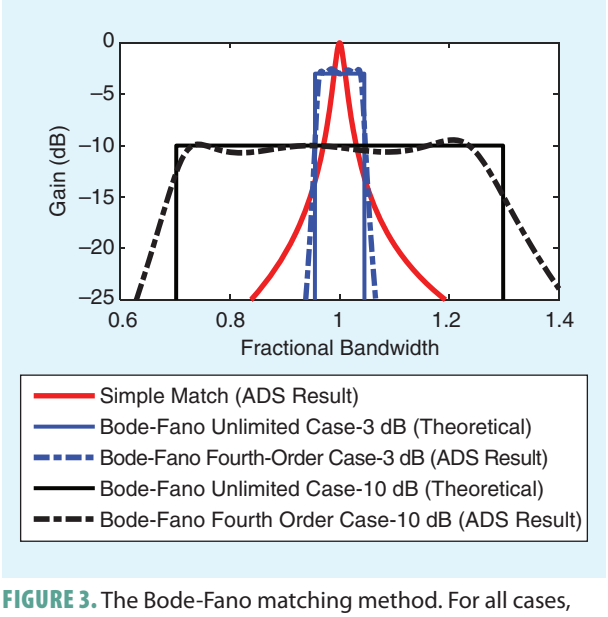

FIGURE 3. The Bode-Fano matching method. For all cases, the unloaded Q-factor is set to 100.

Figure 5 is defined as the available signal-to-noise ratio at the antenna terminal, S_i/N_i, divided by the signal-to-noise ratio delivered to the load, S_o/N_o. Assuming the antenna is lossless and its temperature is $T_A = T_0$, the NF *is* obtained as

$$\mathrm{NF} = \frac{S_i/N_i}{S_o/N_o} = 1 + \frac{\mathrm{NF_{amp}} - 1}{1 - |\Gamma|^2}, \tag{8}$$

where $\mathrm{NF_{amp}}$ and T_0 are the amplifier NF and the room temperature (290 K). Fano's matching network comprises reactive components and does not generate noise. It is lossless, but it is responsible for the realized gain, G_a, and contributes to NF, as seen in (8). In fact, a higher mismatch, $1 - |\Gamma|^2 \to 0$, boosts the effect of the amplifier-generated noise and dramatically deteriorates the overall NF. Nonetheless, it is possible to control the mismatch effect with very-low-noise amplifiers (LNAs), $\mathrm{NF_{amp}} \to 1$. Thus, for the first time, we incorporate the parametric amplifiers as the best candidates for receiving ESA applications to achieve this objective.

While Jacob et al. [12] confirmed the weak noise performance of the non-Foster technique, (8) conceptually verifies that an unfair NF comparison has been made to evaluate the noise performance of the non-Foster technique [7]. Figure 6 (a) and (b) outlines the noise-measurement setup used in [7] to claim the noise performance of the non-Foster technique [see Figure 6(a)] compared with the no-matching (direct-connection) technique [see Figure 6(b)]. Nonetheless, because of two main reasons, none of the corresponding topologies have an advantageous noise characteristic: First, as can be seen in Figure 6(b), there is a large mismatch $(1 - |\Gamma|^2 \to 0)$, between the ESA and Rx due to the high contrast between Z_a and the input impedance of the Rx (50 Ω). As discussed, one can introduce some mismatch to increase the BW. However, it is necessary to use the Bode-Fano theorem [as displayed in Figure 6(c)] to achieve the lowest possible mismatch for a specified BW. Consequently, connecting a high-Q antenna directly to a Rx without matching circuits is not an effective way to increase the BW, and it should not be considered a reference structure for a fair noise comparison. Second, the effect of the active component NF (the amplifier in Figure 5 or Rx in Figure 6) is important due to the mismatch. In case b [see Figure 6(b)], utilizing a high-NF Rx significantly deteriorates the overall NF. Therefore, it would be a more appropriate choice to use an LNA, such as the one displayed in Figure 6(c) for a fair comparison of the NF. We suggest the circuit presented in Figure 6(c) as a proper front end to assess any other matching technique's noise performance.

PRINCIPLES OF THE BROADBAND PARAMETRIC-MATCHING TECHNIQUE

In the previous section, we showed that one needs to introduce mismatch by changing the input impedance of the amplifier to improve the antenna BW. However, we saw an LNA is necessary to keep the noise level low while increasing the BW. This section replaces the amplifier in Figure 6 with a parametric amplifier because it offers lower NF compared to its transistor-based counterpart.

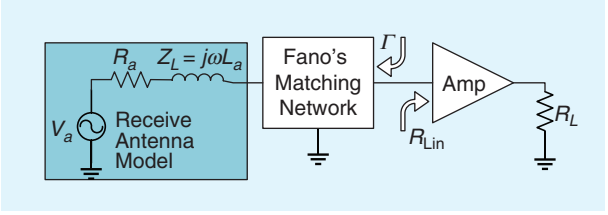

FIGURE 4. The Bode-Fano matching method is attached to an amplifier.

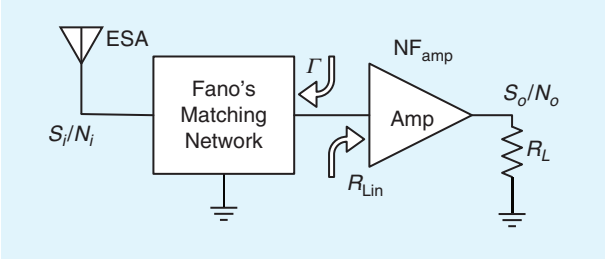

FIGURE 5. The noise characteristics of the Bode-Fano matching method.

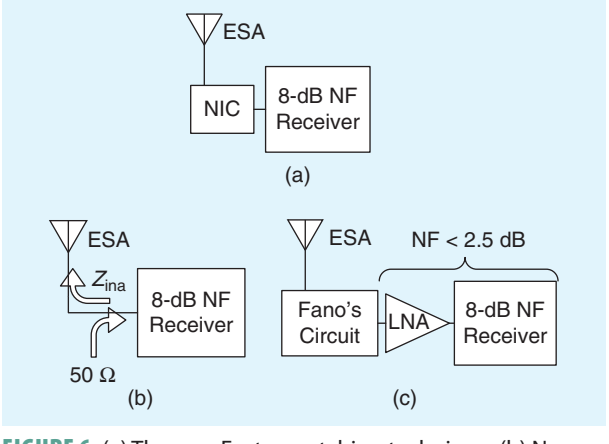

FIGURE 6. (a) The non-Foster matching technique. (b) No matching (direct connection). (c) The Bode-Fano method: 2.5-dB NF is easy to achieve based on the datasheets of the most commercially available LNAs.

REVIEW OF THE UP-CONVERTER PARAMETRIC AMPLIFIER

Figure 7 illustrates the basic topology of the up-converter parametric amplifier consisting of a nonlinear capacitor, $C(v)$, (e.g., a varactor diode) in parallel with three filters at the signal (f_s), pump (f_p), and output (f_o) frequencies [19]. Ideally, each filter would allow current at the associated frequency and would be an open circuit at all other frequencies $(mf_s + nf_p)$. Applying a small-signal voltage, V_a, at f_s, along with a large pumping voltage, V_p, at f_p to the nonlinear capacitor results in a new waveform at the output frequency $(f_o = f_s + f_p)$, which is the amplified version of the input signal, V_a. In Figure 7, R_a, R_P, R_s, and R_L are the signal-source resistance, pump-source resistance, varactor diode loss, and the amplifier load, respectively.

The nonlinear capacitor is modeled as a linear time-variant capacitor using small-signal approximations [19]:

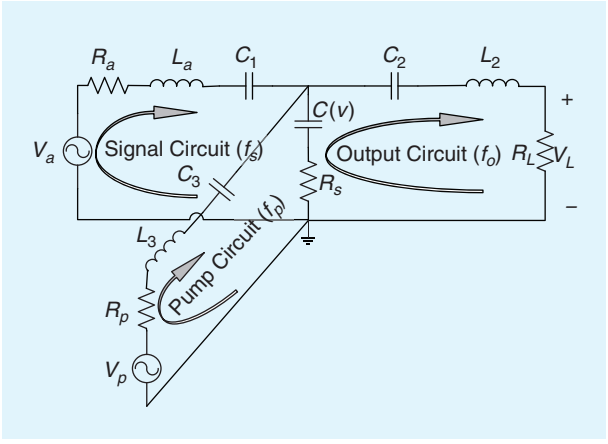

FIGURE 7. The up-converter parametric amplifier. Each loop has zero-net reactance at the associated frequency.

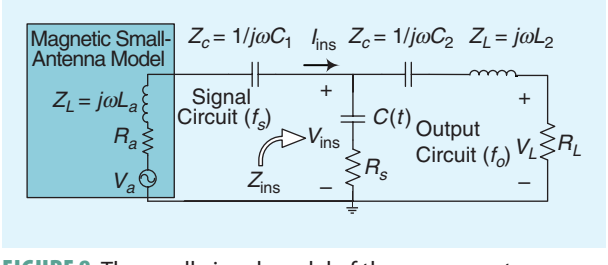

FIGURE 8. The small-signal model of the up-converter parametric amplifier.

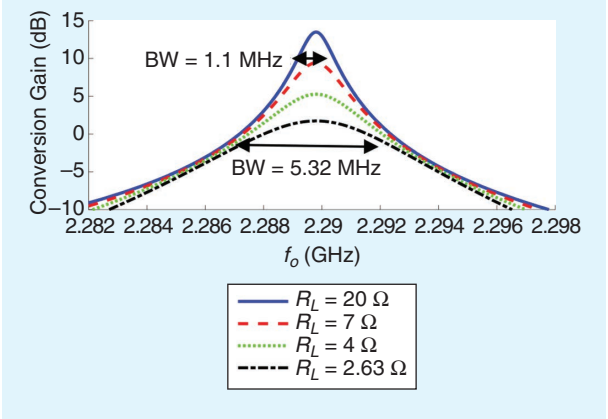

FIGURE 9. The amplifier-conversion gain versus the source resistance (for all graphs, $R_L = R_a$, $C_1 = 0.5$ pF, $C_2 = 0.2$ pF, $C_0 = 4$ pF, $M = 0.23$, $R_S = 0.25\ \Omega$, $L_a = 5.75\ \mu$H, and $L_2 = 25.43$ nH).

$$C(t) = C_0(1 + 2M\cos(2\pi f_p t)), \tag{9}$$

where C_0 and M are the dc-capacitance and the modulation index, respectively. The small-signal model is displayed in Figure 8.

In our work, the series combination of V_a, R_a, and L_a is considered as the circuit model of a magnetic ESA (see Figure 8). The amplifier conversion gain, G_a, is defined as

$$G_a = \frac{\text{Power delivered to } R_L \text{ at } f_o}{\text{Available power from the source at } f_s} = \frac{4R_a V_L^2}{R_L V_a^2}, \tag{10}$$

where V_L is the voltage across the load, R_L. The conversion gain was calculated in [19] using (10) at the midband. Using the same method, we obtain the conversion gain as a function of frequency

$$G_a = \frac{4R_a R_L}{\left| \dfrac{j2\pi f_s(1-M^2)C_0 Z_{TO} Z_{TS}}{M} - \dfrac{M}{j2\pi f_o(1-M^2)C_0} \right|^2}, \tag{11}$$

where

$$Z_{TO} = R_L + R_S + j2\pi f_o L_2 + \frac{1}{j2\pi f_o C_2} + \frac{1}{j2\pi f_o(1-M^2)C_0}$$

$$Z_{TS} = R_a + R_S + j2\pi f_s L_a + \frac{1}{j2\pi f_s C_1} + \frac{1}{j2\pi f_s(1-M^2)C_0}.$$

WIDEBAND MATCHING TECHNIQUE

f_s and f_o must be specified to design the up-converter parametric amplifier. We selected $f_s = 100$ MHz and $f_o = 2{,}290$ MHz. The design parameters are given in the caption of Figure 9. The amplifier conversion gain is computed using (11) for $R_L = R_a = 20\ \Omega$ (maximum gain condition). The conversion gain is displayed with the solid line in Figure 9. As depicted, the output-stage BW (BW = 1.1 MHz) is almost doubled compared to the input-stage unloaded resonator BW, defined as

$$\Delta f_S = \frac{f_S}{Q_S} = \frac{R_a}{2\pi L_a}, \tag{12}$$

where Q_S is the Q-factor of the input stage resonator (Chu's Q-factor for the receiving antenna model). The impedance seen by the signal circuit toward the time-variant capacitor at f_s is

$$Z_{\text{ins}} = \frac{V_{\text{ins}}(f_s)}{I_{\text{ins}}(f_s)}, \tag{13}$$

where V_{ins} and I_{ins} are the voltage and current of the time-varying capacitor at f_s, as illustrated in Figure 8. One can compute the real part of the impedance at the midband [19] frequency as

$$R_{\text{ins}} = \text{Re}[Z_{\text{ins}}] = R_s + \frac{M^2}{4\pi^2 f_s f_o C_0^2 (1-M^2)^2 (R_L + R_S)}. \tag{14}$$

R_{ins} is a positive quantity because $M < 1/2$. As a result, the up-converter parametric amplifier is inherently a stable device in contrast to the non-Foster technique. R_{ins} loads the input circuit, and the modified (loaded) BW of the input-circuit resonator is defined as

$$\Delta f_{SL} = \frac{f_S}{Q_{SL}} = \frac{(R_a + R_{\text{ins}})}{2\pi L_a}, \tag{15}$$

where Q_{SL} is the Q-factor of the loaded input circuit (receive antenna). For the maximum gain condition (matched case), R_{ins} is equal to R_a, resulting in $\Delta f_{SL} = 2\Delta f_S$, which explains why the overall signal BW is twice the BW of the unloaded resonator in the input circuit for the maximum-gain condition.

According to (14) and (15), reducing the load resistance, R_L, increases R_{ins}, thus, reducing the loaded quality factor of the input circuit and increasing its BW. Figure 9 demonstrates

the amplifier conversion gain calculated using (11) for different R_L values ($R_L = R_a$) while other parameters are fixed. As presented, reducing R_L decreases the conversion gain of the amplifier due to the mismatch between R_a and R_{ins}, leading to an increase in the BW in accordance with the Bode-Fano theorem. We used the first-order Bode-Fano circuit to simplify the equations.

Mismatch lowers the received signal level, resulting in the degradation of the overall NF of the Rx. However, the overall NF in the suggested approach is still limited due to two primary factors: 1) The antenna is a part of the amplifier circuit that allows the removal of the loss of the transmission line between the antenna and the amplifier and 2) the parametric amplifier is naturally a low-noise device.

We define BW enhancement as the amplifier BW divided by twice of the BW of the unloaded resonator in the input circuit (BW/2Δf_s). Figure 10 displays the BW enhancement and conversion gain of the amplifier versus R_L. As seen, a BW improvement of 32 times is observed for $R_L = R_a = 2.63\ \Omega$, corresponding to a total conversion gain of 2 dB. (The parametric amplifier conversion gain was compensated for the mismatch loss.)

NOISE CONSIDERATIONS

The NF of the up-converter parametric amplifier is defined as

$$\mathrm{NF} = \frac{N_o}{N_i G_a}, \tag{16}$$

where N_o is the output-noise power delivered to the load as a result of noise generated by R_a at f_s and noise generated by R_s at f_s and f_o. The NF of the up-converter parametric amplifier at midband frequency has been derived from [19]. We use the same method to formulate the NF versus frequency in the entire BW. Figure 11 plots the NF for different values of $R_L = R_a$. As depicted, the NF is lower than 3 dB in the entire 3-dB BW when $R_L = R_a = 2.63\ \Omega$, corresponding to a BW enhancement of 32 times.

REALIZED ANTENNA DESIGN AND HIGH-FREQUENCY STRUCTURE SIMULATOR SIMULATIONS

We have considered the primary circuit models for the antenna (see Figure 4) and parametric amplifier (see Figure 7). Although circuit models are ideal and do not include parasitic effects (e.g., the loss associated with input and output circuits), they helped us to formulate the entire structure based on the closed-form equations. In this section, the idea is further developed by proposing a realized parametric amplifier circuit (see Figure 12) and a realized received-antenna model (see Figure 13). These realized structures are modeled and simulated considering all nonideal effects, including the parasitic elements.

CIRCUIT DESIGN

In the previous sections, lumped inductors and capacitors have been utilized to implement filters (series *LC*-resonators as displayed in Figure 7). In practical designs, the limited Q-factor of lumped components makes them lossy, leading to deteriorating the overall NF. Also, it was assumed that each filter is an open circuit at all frequencies other than its resonant frequency, which is hard to accomplish using the basic circuit displayed in Figure 7. To address these issues, distributed filters and matching circuits were utilized in the design, as depicted in Figure 12.

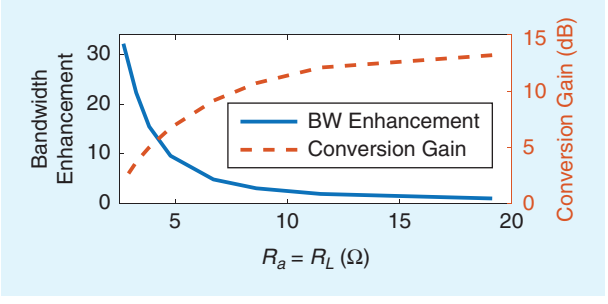

FIGURE 10. The amplifier-conversion gain and BW enhancement versus the source resistance (for all graphs, $R_L = R_a$).

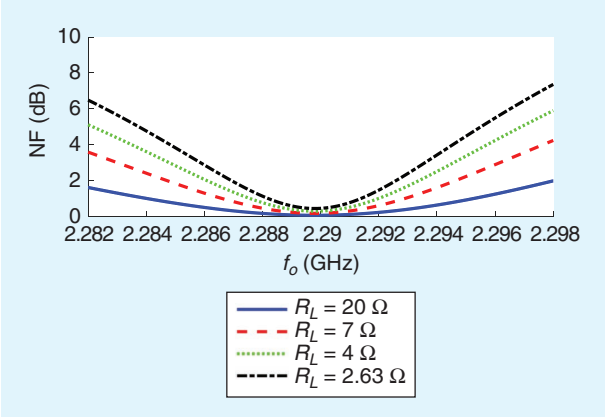

FIGURE 11. The NF versus the source resistance (for all graphs, $R_L = R_a$).

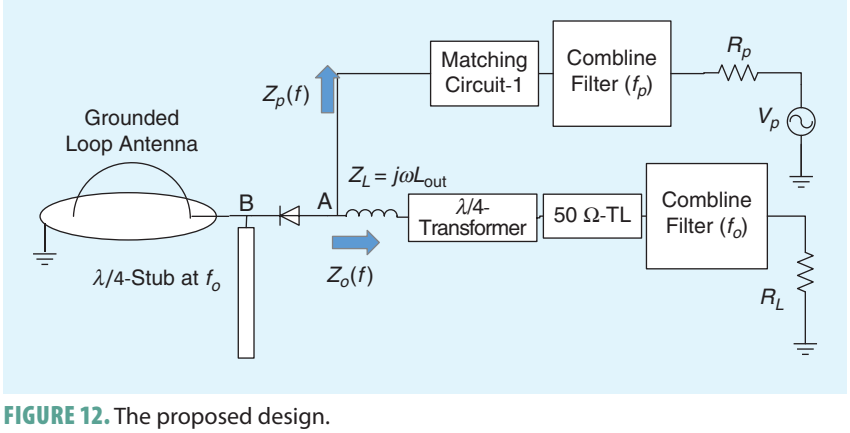

FIGURE 12. The proposed design.

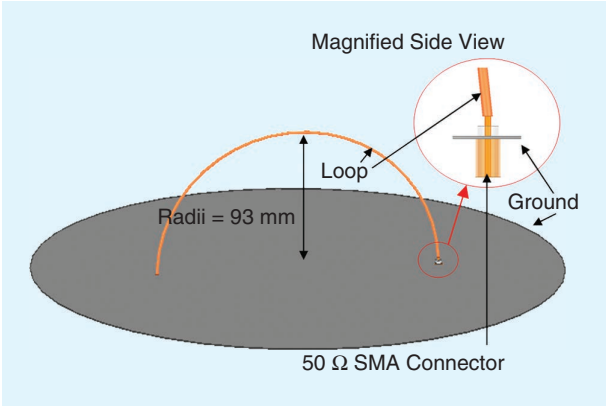

FIGURE 13. The grounded electrically small-loop antenna.

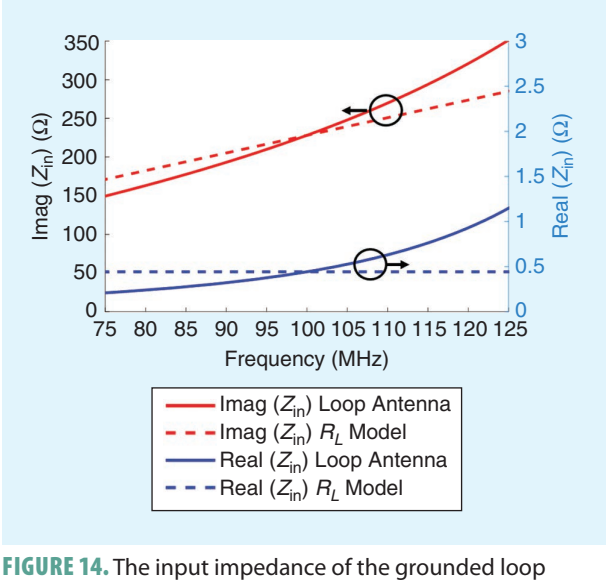

FIGURE 14. The input impedance of the grounded loop antenna.

We briefly discuss the general idea of the design by comparing the basic topology (the circuit model illustrated in Figure 7) of the parametric amplifier and the proposed design (see Figure 12) in the following paragraphs.

First, LC-resonators (filters) at the output (L_2C_2) and pump (L_3C_3) circuits are replaced with two combline filters, offering high rejection while keeping the passband loss minimum. Simulation results show that the input impedance of the combline filter is purely inductive and very small at f_s ($\ll f_o$ or f_p), making it almost short-circuit at f_s. However, as required by the basic topology in Figure 7, the output and pump circuits needed to be open circuit at f_s. Otherwise, they load the nonlinear capacitor at f_s and deteriorate the performance of the amplifier. To overcome this issue, the varactor diode is placed in series with the signal circuit in the new design, as depicted in Figure 12. This way, node A in Figure 12 is shorted out at f_s, and the dc capacitance of the varactor diode resonates directly with the antenna inductance at f_s, leading to a removal of C_1 from the original design. However, an $\lambda_o/4$ open-circuited stub is incorporated in the signal subcircuitry to make node B almost short-circuited at both f_o and f_p frequencies and close the loops of the output and pump circuits. Note that the $\lambda_o/4$ open-circuited stub behaves like a small capacitor at f_s and has a negligible effect on the performance of the input circuit.

Matching circuit-1 is utilized to match the pump source at f_p and make the pump circuit transparent to the output circuit at f_o by making $Z_p(f_o)$ very large (almost open-circuit). Finally, the $\lambda/4$-transformer and L_{out} in the output subcircuitry are incorporated to adjust the real and imaginary parts of the input impedance of the output circuit, $Z_o(f_o)$, to the values required by the up-converter parametric amplifier design.

GROUNDED ELECTRICALLY SMALL LOOP ANTENNA

A grounded electrically small-loop antenna is incorporated as a realized antenna to validate the proposed design. The antenna structure is depicted in Figure 13.

The antenna is simulated using the high-frequency structure simulator (HFSS), and its input impedance is plotted in Figure 14, which shows that the input impedance is highly reactive. Simple RL model [see Figure 2(a)] for the grounded-loop antenna is obtained by equating the input impedance of the RL-circuit model and the antenna-input impedance at the exact frequency of 100 MHz. As seen, the simple RL circuit does follow the curves associated with both imaginary and real parts of the antenna-input impedance, where the frequency approaches the resonant frequency, and this is not an accurate model. To have a better model, one can consider Chu's circuit for the first mode, TE_{10}. However, in the remaining part of the article, we use the exact model of the antenna computed by HFSS.

COMBLINE FILTERS' DESIGN AND SIMULATIONS

Care must be taken in the design of combline filters because they affect the performance of the proposed design in different ways. First, since the output combline filter defines the loss in the output circuit, its insertion loss directly contributes to the overall NF. Thus, the insertion loss of the output combline filter (at f_o) should be as low as possible. Second, the pump combline filter should highly reject the noise of the pump circuit at f_s and f_o. Otherwise, the noise of the pump source is injected into the output circuit and deteriorates the overall NF. Third, although the insertion loss of the pump filter at f_p does not contribute to the overall NF, it defines the efficiency of the pump circuit.

Fifth-order combline filters centered at f_o and f_p are designed using the procedure described in [20] and [21]. The output combline filter is designed to be wideband (leading to a low insertion loss) while the pump combline filter is designed to be narrow-band, resulting in a high rejection at f_o while having a moderate insertion loss. Figure 15 presents the structure simulated in the HFSS. As depicted in Figure 16(a), the passband insertion loss of the output filter centered at $f_o = 2.29$ GHz and pump filter centered at $f_p = 2.19$ GHz are 0.3 dB and 1 dB, respectively. The output filter rejection at $f_p = 2.19$ GHz and pump filter rejection at $f_o = 2.29$ GHz are simulated to be 40 dB and 80 dB, respectively. Thus, the pump-to-output port isolation is more than 40 dB and 80 dB at f_p and f_o, respectively.

Figure 16(b) illustrates the input impedance of both combline filters around the signal frequency. As shown, the real part is close to zero, and the imaginary part has a small inductive value around $4j\,\Omega$ at $f_s = 100$ MHz. It does not alter these properties across the signal frequency by connecting other passive components in the output and pump subcircuits (including matching network-1, L_{out}, and $\lambda/4$-transformer) to the combline filters. Then, input impedance seen by the signal circuit toward pump and output circuits at f_s [defined as $(Z_o(f_s) \times Z_p(f_s))/(Z_o(f_s) + Z_p(f_s))$] in Figure 12] has a real part close to zero and a small inductive imaginary part. In other words, pump and output circuits load the signal circuit at f_s by small inductive impedance, leading to a slight detuning of the resonant frequency of the signal circuit. The resonant frequency can be tuned again by adjusting the dc bias of the varactor diode. As a result, point A in Figure 12 can be assumed as a virtual ground (or, more accurately, as a small inductive load) for the signal subcircuit at f_s.

THE ACTUAL MODEL OF THE VARACTOR DIODE

The MA46H2020 varactor diodes from MACOM technology solutions are chosen as the active components. Two varactor diodes are connected in parallel to lower equivalent series resistance, which is the primary source of noise in the proposed design. The procedure explained in [19] and [22] and the nonlinear capacitance-voltage characteristics (extracted from the datasheet of MA46H2020) are used to extract C_0 and M associated with the time-variant model [see (9)] of the two diodes in parallel.

Figure 17 depicts C_0 and M versus the pump peak voltage for two different dc biases applied to the varactor diodes. An increase in the reverse dc bias decreases the dc capacitance, evident from the diode's C-V curve. Also, Figure 17 presents that the modulation index increases by increasing the pump voltage. It is worth mentioning that the data extracted from plots like the one in Figure 17 and the concepts explained in the "Principles of the Broadband Parametric Matching Technique" section help us evaluate the general behavior of the amplifier and choose the varactor diode.

FEED NETWORK

So far, the design of two combline filters and grounded loop antenna has been explained. Other parts of the proposed design (see Figure 12) are implemented on a single-layer RT/duroid 5880 printed circuit board which is illustrated in Figure 18. A small piece of wire in the output circuit is used as the output inductor, $L_{out} \approx 1$ nH. Ports one, two, and three of the feed network are connected to the antenna, output combline filter, and pump combline filter, respectively. Other parts are implemented as explained in the "Circuit Design" section.

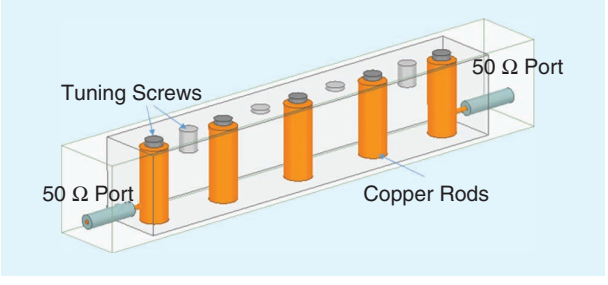

FIGURE 15. The combline filter designed at f_o.

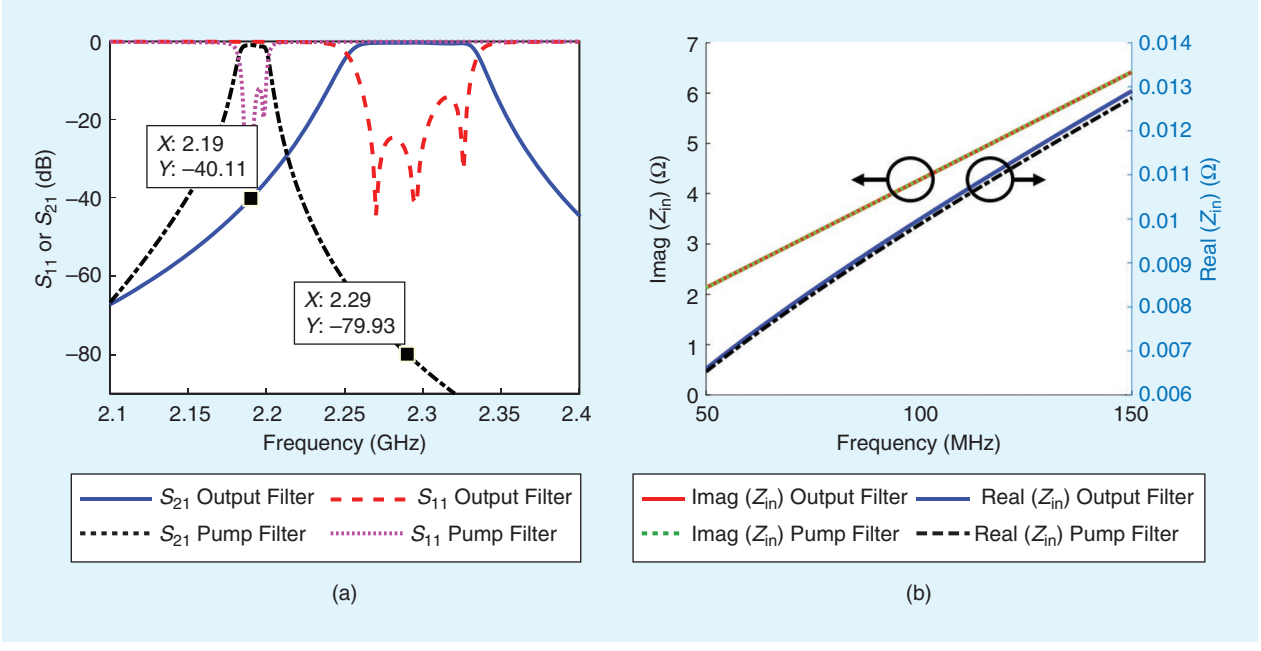

FIGURE 16. (a) The scattering parameters of the combline filters around the pump and output frequencies. (b) The input impedance of the combline filters around the signal frequency.

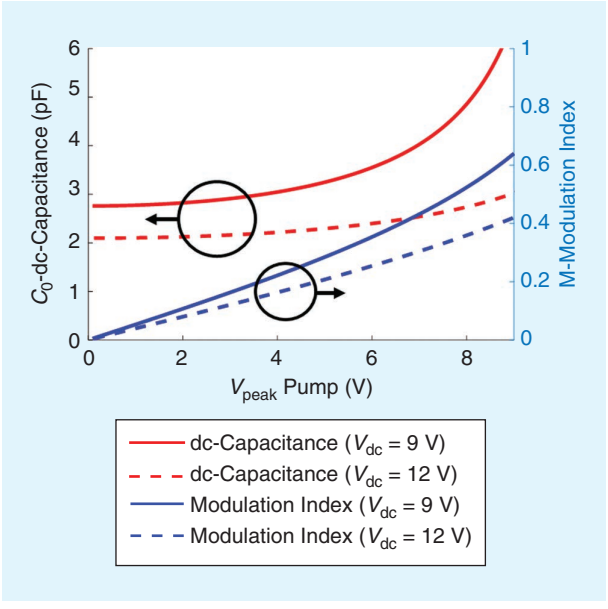

FIGURE 17. The time-variant capacitor parameters versus the pump voltage.

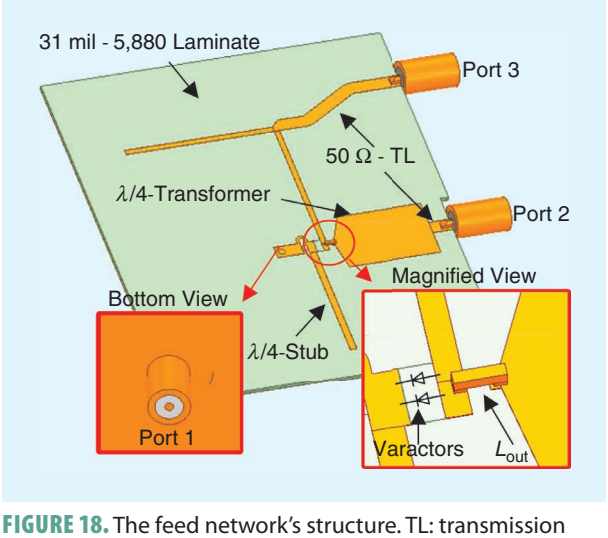

FIGURE 18. The feed network's structure. TL: transmission line; 1 mil: one-thousandth of an inch.

HYBRID SIMULATIONS OF THE REALIZED STRUCTURE

Hybrid simulation (HFSS+ADS) is performed on the proposed design to investigate the nonlinear behavior. First, as a transmit antenna, a small dipole antenna is placed 1 m away from the grounded loop antenna, as a receive antenna, and the entire structure (two-ports network) is simulated in the HFSS. Then, the varactor diodes in Figure 18 are replaced with a lumped port (port four), and HFSS is used to simulate the entire feed network (four-ports network).

The parametric amplifier is a nonlinear device that generates all $mf_s + nf_p$ components. To accurately model the structure, all passive components (including combline filters, the feed network, and the antenna element) need to be simulated in a wide range of frequencies. Accordingly, throughout this article, all passive components are simulated in the range of 50 MHz to 8 GHz.

To investigate the BW performance, we swept the input frequency from 92 MHz to 108 MHz and captured the output power or noise in the frequency range of 2,282 MHz to 2,298 MHz (the pump waveform was a single-tone at 2,190 MHz). Accordingly, the gain and/or noise of the proposed design may be reported versus f_o or $f_s\,(=f_o-f_p)$. Throughout the article, the simulated results of the proposed design were plotted versus f_s whenever they needed to be compared to the reference structure. Note that both the input and output waveforms of the reference structure were centered at $f_s = 100$ MHz.

In the next step, scattering parameters were imported to the ADS software to perform harmonic balance (HB) simulations, as detailed in Figure 19. In this setup, the dipole antenna was fed by a 50-Ω source as a Tx, and, on the receive side, the loop antenna was connected to port one of the feed network. Two varactor diodes in parallel were connected to port four of the feed network. As displayed, parasitic elements associated with the package of the varactor were considered in the simulations. Finally, the output and pump combline filters were connected to port two and port three of the feed network. It is worth mentioning that the noise and gain results of the ADS simulations include all parasitic effects (including the loss associated with the diodes, combline filters, and feed network) because the scattering parameters of the entire lossy structure were computed using a full-wave simulation (HFSS).

To investigate the BW improvement of the proposed method, another simulation for the simple matched load case was set up in the ADS. In this simulation, the same receiving loop antenna was directly connected to the matched load, as depicted in Figure 1(a). The received power by the matched load was normalized to 0 dB and is depicted in Figure 20. On the other hand, the received power by the 50-Ω load in the proposed method was not normalized to 0 dB but was plotted relative to the received power by the matched load. Although the proposed design receives power at $f_o = 2.29$ GHz, in Figure 20, it is plotted versus $f_s\,(=f_o-f_p = 100\text{ MHz})$ to have both plots in the same figure for the BW comparison. As depicted, the 3-dB BW of the proposed method has been improved 26.5 times compared to the simple matched case. However, for the *RL* circuit model described in the "Principles of the Broadband Parametric Matching Technique" section, we got a BW enhancement of a magnitude of 32. The small difference is due to using the simplified *RL* model in the "Principles of the Broadband Parametric Matching Technique" section, and our simulations show that using Chu's exact circuit model leads to a BW enhancement of a magnitude of 26.5 times.

Note that, according to the circuit presented in Figure 4, it is possible to increase the BW utilizing a transistor amplifier as well. Therefore, a first-order Bode-Fano circuit was designed and was connected to an amplifier block in the ADS. The gain and impedance of the amplifier block are defined as 13.5-dB and 50-Ω, respectively. The NF of the amplifier

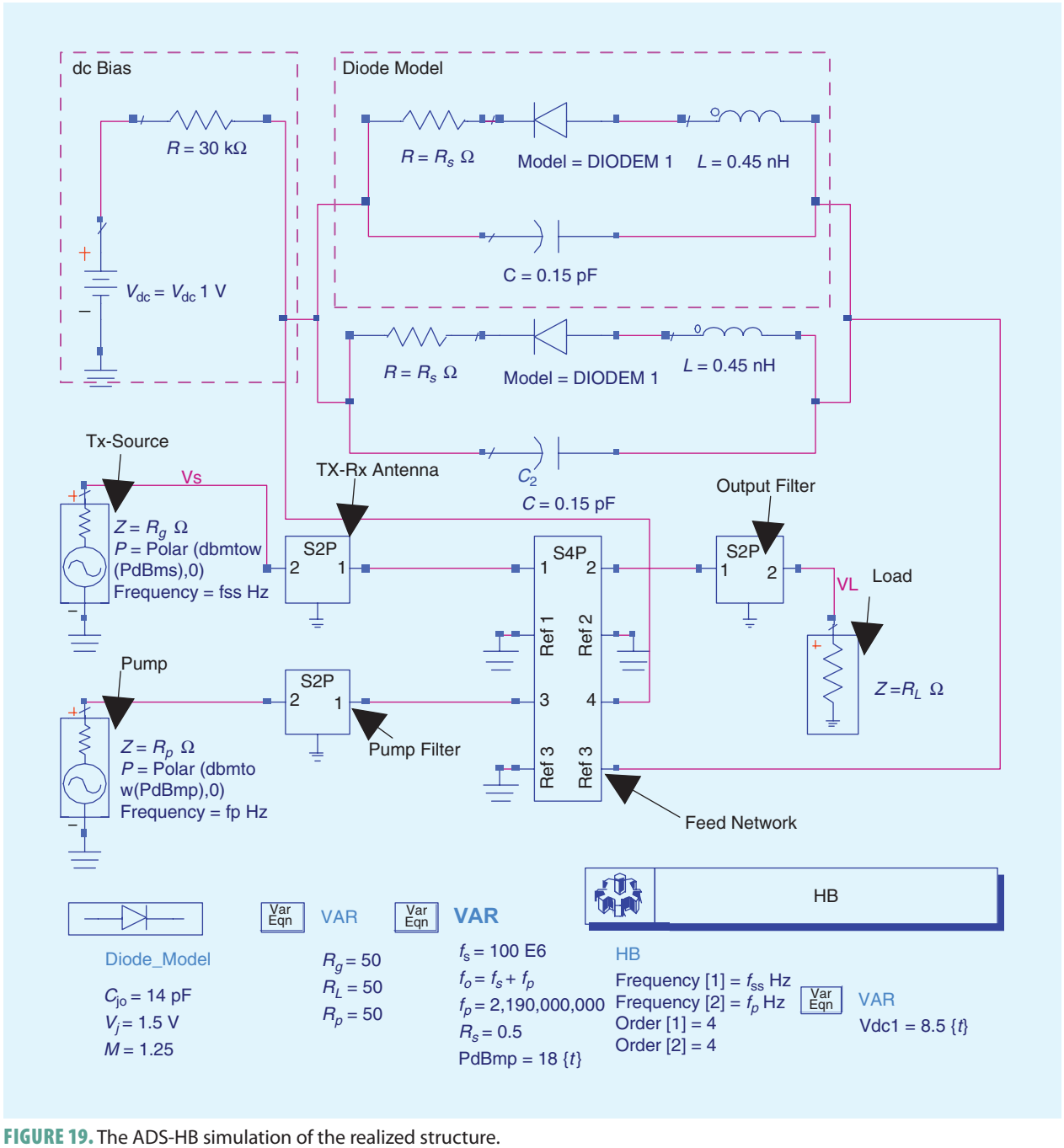

FIGURE 19. The ADS-HB simulation of the realized structure.

block was set to 0.5 dB, 0.75 dB, or 1 dB, which are the typical values for the low-noise transistor amplifiers in the market. The mismatch between the antenna and the amplifier block was adjusted to get the BW like the proposed design to have a fair noise comparison. Also, the same antenna and the transmit power were used for the amplifier-block simulations. The received power (by $R_L = 50\ \Omega$ in Figure 4) is plotted in Figure 20. Again, the received power was not normalized to 0 dB and is plotted relative to the received power by the matched load. As displayed, the 3-dB BW in the case of the amplifier block and the parametric amplifier are almost the same.

The noise simulations for the parametric up-converter and conventional amplifier block were performed in the ADS. In both cases, the effect of the antenna loss in the overall NF was ignored because it added the same value to the overall NF of both cases. The overall NFs, including the effect of mismatch, are illustrated in Figure 21. As displayed, the NF of the antenna connected to the up-converter active part was 2.9 dB lower than the same antenna connected to an extremely low LNA (e.g., NF = 0.5 dB). It is worth mentioning that a lossless capacitor and feeding structure was used to design a first-order Bode-Fano circuit in the amplifier block case. As a result, the actual

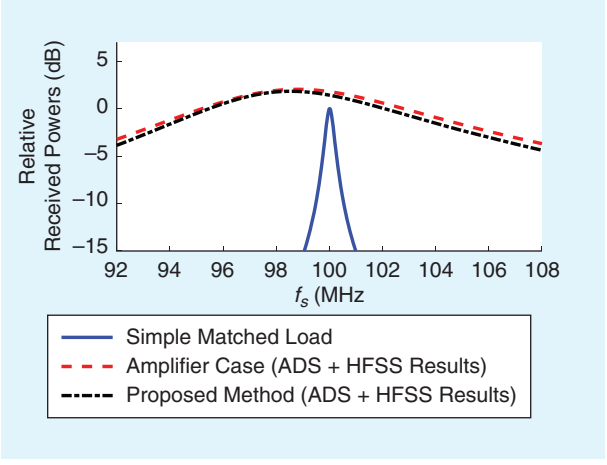

FIGURE 20. The relative received powers by the simple matched load case, the proposed method, and the amplifier block. For all cases, the transmit power and the receiving loop antenna are the same. The simple matched load case and amplifier-block case receive power at f_s while the proposed method receives power at $f_o = f_p + f_s$.

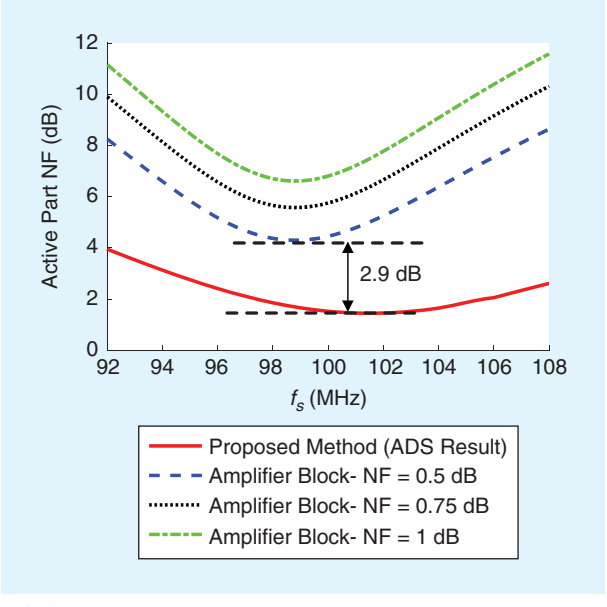

FIGURE 21. The overall NF comparison. The NF for the amplifier block is simulated and plotted at $f_s = 100$ MHz while for the proposed structure is simulated at $f_o = 2.29$ GHz and is plotted versus $f_s = f_o - f_p = 100$ MHz.

NF for the realized conventional amplifier block case would be higher. However, the varactor diode (MA46H2020) used in the parametric amplifier (MA46H2020) is a commercially available component.

The pump power and dc bias are set to 18 dBm and 8.5 volts. Considering an efficiency of about 11% for the pump circuitry (including the pump filter loss, synthesizer dc power consumption, and so on), the total power consumption of the proposed structure is 582 mW. The parametric amplifier does not consume any power from the dc source because of a zero-dc current. Similar ADS simulations have been performed for other methods, which are outlined in Figure 1, and the results are compared to the proposed active matching technique in Table 1. The TQP3M9036 transistor amplifier from Qorvo is considered as the load for all cases, and its parameters (NF, input P1dB, and so on) are imported in the simulations.

TABLE 1. A COMPARISON BETWEEN OUR DESIGN AND OTHER METHODS.

Method \ parameter	BW (MHz)	NF (dB)	Power (mW)	P1dB (dBm)	IIP3 (dBm)
Proposed design [Figure 1(d) + parametric amplifier]	10	1.45	582	−15	−4.5
Tuned mismatch case [Figure 1(d) + TQP3M9036 amplifier]	10	4.3	340	−8	+2
Adding loss [Figure 1(b) + TQP3M9036 amplifier]	11	15.5	340	−8	+2
Direct connection [Figure 1(c) + TQP3M9036 amplifier]	18	13.5	340	−8	+2

As seen, the proposed technique has the best noise performance while direct connection has the maximum BW. The received power for the direct connection case increases by frequency (due to an increase in the antenna electrical size), and its BW is defined as a 3-dB variation around 100 MHz. Furthermore, as discussed, [12] confirms that the direct connection case is better than the non-Foster technique. As illustrated in Table 1, compared to the transistor counterpart, the parametric amplifier needs higher power to operate, and it offers a lower-input P1dB compression point and IIP3.

THE PROTOTYPED STRUCTURE AND MEASUREMENTS

The proposed active matching system has been prototyped at the Virginia Tech Antenna Group Laboratory. Figure 22 presents one of the prototyped combline filters. Aluminum tubes and sheets were used to make the housing while copper rods were used as resonators. Combline filters of pump and output circuits were tuned using tuning screws. Scattering parameters were measured using the Rohde & Schwarz (R&S) ZVA50 vector-network analyzer and are displayed in Figure 23 along with the simulated results. A small discrepancy between simulated and measured results exists due to handmade prototyping tolerances. However, the critical parameter in our design is the insertion loss, which is acceptable and measured to be 0.55 dB and 1.9 dB for the output filter and the pump filter, respectively.

In the next step, the grounded loop antenna and the feed network were prototyped, and all of the parts were assembled. As displayed in Figure 24, the antenna port was connected to

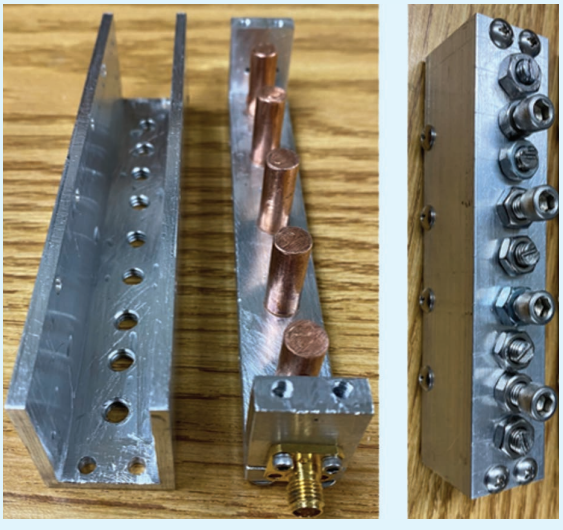

FIGURE 22. The prototyped combline filter at the output circuit.

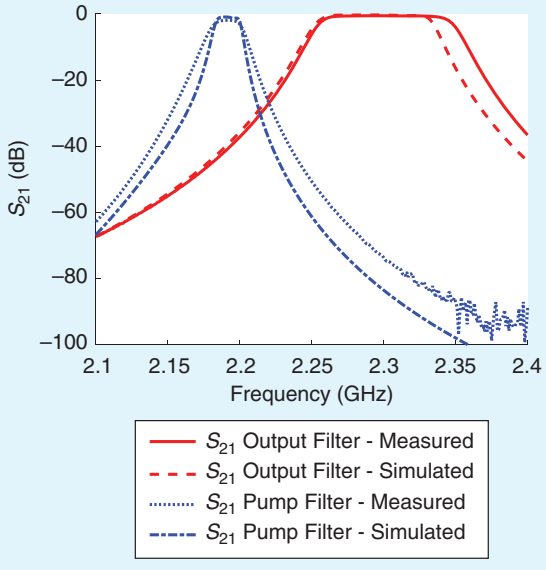

FIGURE 23. The frequency responses of the combline filters.

port one of the feed network while port two and three of the feed network were connected to the output and pump filters.

A measurement set up, as presented in Figure 25, was implemented to evaluate the antenna performance. In this setup, a small monopole antenna was connected to the Tektronix AFG3252 signal generator to form a transmit system. The prototyped structure was configured as a Rx antenna, and an R&S FSU spectrum analyzer measured its output power spectrum. The entire structure was placed inside an anechoic chamber, and the distance between the Tx and Rx antennas was about 4 m. Simultaneously, a dc source and an HP 8648 D signal generator were connected to the amplifier as the dc-bias and pump source. The pump-source frequency, f_p, was set to 2.19 GHz while the Tx frequency, f_s, swept from 92 MHz to 108 MHz. As presented in Figure 17, increasing the dc bias of the varactor diode decreased its dc capacitance, reducing the resonance frequency. This property was utilized to fine-tune the structure, leading to the dc bias of 8.75 V. Finally, the pump power was adjusted to different levels, and the received power spectrums are plotted in Figure 26. As displayed, about 10% (10-MHz) BW was obtained for the pump's available power of 138 mW (21.4 dBm). Although the HP 8648 D was used as a pump source, in the final structure, the LX2531 synthesizer from Texas Instruments and the QPA9120 driver amplifier from Qorvo could be used to inject 21.4 dBm at f_p to the structure. By adding the power consumptions of the LMX2531 synthesizer and QPA9120 amplifier, the overall power consumption of the proposed design was obtained to be 582 mW.

For comparison, a reference setup is implemented by replacing the proposed structure with a grounded passive-loop antenna of the same size as the antenna in our design. The passive-loop antenna is matched to 50 Ω and is connected to the spectrum analyzer while the Tx system and its transmit power stays the same. The BW of the passive antenna is measured to

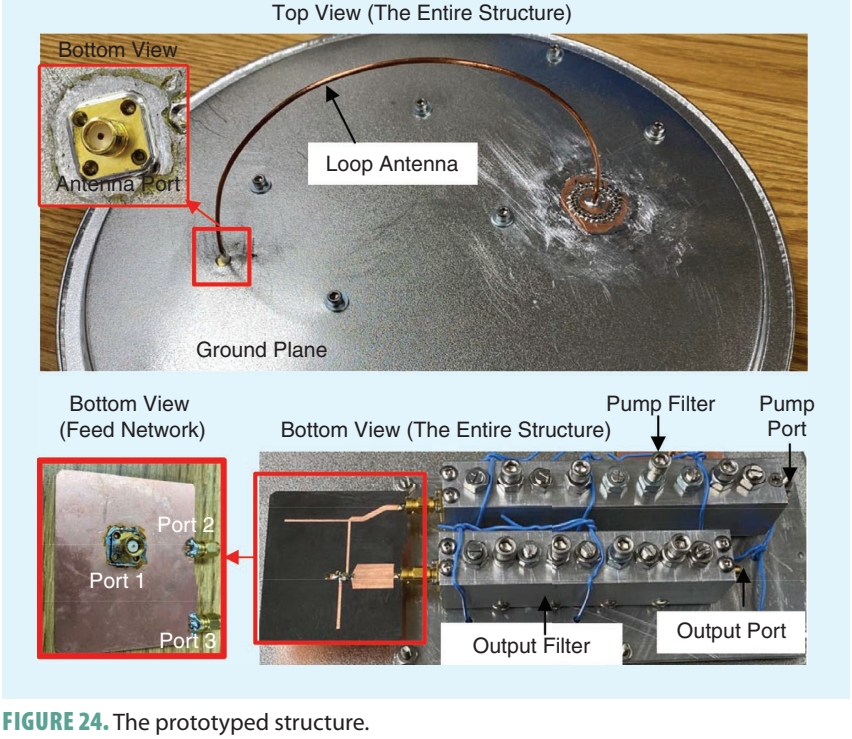

FIGURE 24. The prototyped structure.

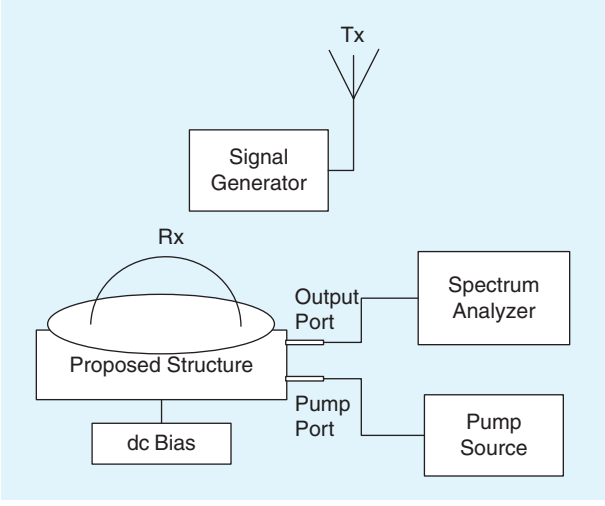

FIGURE 25. The test setup.

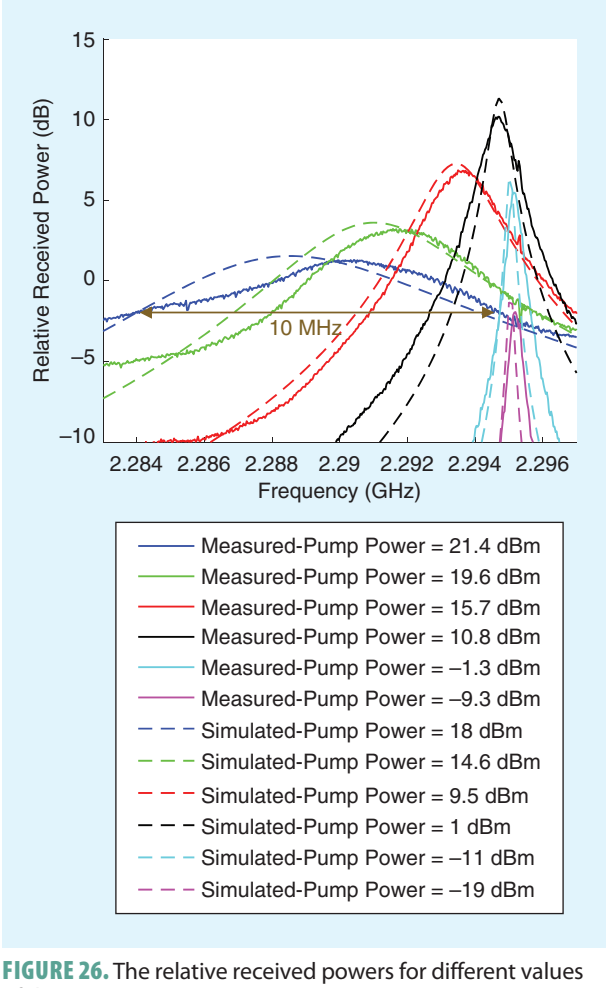

FIGURE 26. The relative received powers for different values of the pump power.

be 0.55 MHz, leading to BW enhancement of a magnitude of 18 of that in the prototyped structure. Note that the measured plots in Figure 26 are relative to the received power by the simple passive matched case. As depicted, the measured Rx gain (parametric amplifier gain + mismatch loss) was 10.2 dB for the matched case corresponding to the maximum-gain condition (the solid black line in Figure 26) while it was measured to be 1.25 dB for the 10-MHz-BW case (the solid blue line in Figure 26).

The relative simulated results are also included in Figure 26. As depicted, the same trend exists in both the simulated and measured results when we increase the pump power. This trend is explained using the circuit model displayed in Figure 8. For very small values of pump power, M is close to zero (see Figure 17), and, based on (14), the input impedance of the time-variant capacitor, R_{ins} (see Figure 8) at f_s is significantly smaller than the source resistance, R_a, leading to a large mismatch between the source and time-variant capacitor. As a result, the conversion gain is small, and the receiving BW is narrow. Increasing the pump power (increasing M), increases R_{ins}, and, for some specific value of the pump power, R_{ins} becomes equal to R_a, leading to the maximum-gain condition. In this case, the input and output ports of the parametric amplifier were matched to the source and load, respectively, and the voltage standing-wave ratio of input and output ports is close to 1. Further increasing the pump power makes R_{ins} larger than R_a, leading to a widening of the signal BW [see (15)] at the expense of mismatch and gain reduction.

Another trend in Figure 26 is the change in the resonance frequency. According to Figure 17, increasing the pump power increases the dc capacitance of the varactor diode, leading to a shift down the resonant frequency, as depicted in Figure 26.

As detailed in Table 1, the measured P1dB and IIP3 of the proposed structure are –4.5 dBm and –15 dBm, respectively. To measure IIP3, two small monopoles were connected to two sources as the two-tone test Tx. Another important parameter in the design of a parametric amplifier (same as the mixer design) is the isolation between different ports. Table 2 summarizes the measured port to port isolations. As seen, due to the use of the combline filters, an 85.5-dB isolation was obtained between the pump port and the output port at f_o, meaning that the noise generated by the pump source was suppressed in the output port. Also, a 44.5-dB isolation was achieved between the same ports at f_p, leading to a suppression of the pump components in the output port.

Due to the high level of ambient noise in the vicinity of f_s, we were not able to measure and validate the noise performance

TABLE 2. MEASURED ISOLATION BETWEEN DIFFERENT PORTS.

Frequency	f_s	f_p	f_o
Pump-Output Isolation (dB)	—	42.9	85.5
Antenna-Pump Isolation (dB)	More than 110	44.5	98
Antenna-Output Isolation (dB)	More than 110	61.4	–24.8

of the prototyped structure. However, we relied on the simulated results (see Figure 21) to validate the noise performance of the design. Furthermore, Figure 26 confirms the good agreements that exist between the simulated and measured received powers for different situations (e.g., the pump power level). As a result, the noise performance of the prototyped structure should not depart from the simulated results.

CONCLUSIONS

A review of the Bode-Fano bound and Chu's limits were given in the context of the ESA as an *RLC* [see Figure 2(b)] resonator. Then, a low-noise wideband impedance matching technique was introduced for ESAs. First, theoretical outcomes were compared to the circuit-model simulations. Then, the circuit model was converted to a distributed model, and full-wave simulations of the realized structure were conducted. The overall NF of the structure was compared to the transistor case to show the effectiveness of the proposed method. Incorporating a higher-order Bode-Fano circuit would improve the NF in both transistor and up-converter cases. However, in this article, we used the first-order Bode-Fano circuit to simplify the problem and conceptually explain the effectiveness of the method. Finally, the structure was prototyped, and measured received signals were compared to the simulated ones.

AUTHOR INFORMATION

Pedram Loghmannia (pedraml@vt.edu) is a senior design engineer with Qorvo, Inc, Apopka, Florida, 32703, USA. He is a Student Member of IEEE.

Majid Manteghi (manteghi@vt.edu) is an associate professor with the Bradley Department of Electrical and Computer Engineering, Virginia Polytechnic Institute and State University, Blacksburg, Virginia, 24061, USA. He is a Senior Member of IEEE.

REFERENCES

[1] L. J. Chu, "Physical limitations of omni-directional antennas," *J. Appl. Phys.*, vol. 19, no. 12, pp. 1163–1175, 1948. doi: 10.1063/1.1715038.

[2] H. A. Wheeler, "Fundamental limitations of small antennas," *Proc. IRE*, vol. 35, no. 12, pp. 1479–1484, 1947. doi: 10.1109/JRPROC.1947.226199.

[3] R. M. Fano, "Theoretical limitations on the broadband matching of arbitrary impedances," *J. Franklin Inst.*, vol. 249, no. 1, pp. 57–83, 1950. doi: 10.1016/0016-0032(50)90006-8.

[4] M. Manteghi, "Fundamental limits, bandwidth, and information rate of electrically small antennas: Increasing the throughput of an antenna without violating the thermodynamic Q-factor," *IEEE Antennas Propag. Mag.*, vol. 61, no. 3, pp. 14–26, 2019. doi: 10.1109/MAP.2019.2907892.

[5] H. Wolff, "High-speed frequency-shift keying of LF and VLF radio circuits," *IRE Trans. Commun. Syst.*, vol. 5, no. 3, pp. 29–42, 1957. doi: 10.1109/TCOM.1957.1097513.

[6] M. Manteghi, "An electrically small antenna concept design for transmitting a baseband signal," in *Proc. IEEE Int. Symp. Antennas Propag. & USNC/URSI Nat. Radio Sci. Meeting*, July 9–14, 2017, pp. 1481–1482. doi: 10.1109/APUSNCURSINRSM.2017.8072783.

[7] S. E. Sussman-Fort and R. M. Rudish, "Non-Foster impedance matching of electrically-small antennas," *IEEE Trans. Antennas Propag.*, vol. 57, no. 8, pp. 2230–2241, 2009. doi: 10.1109/TAP.2009.2024494.

[8] N. Zhu and R. W. Ziolkowski, "Active metamaterial-inspired broad-bandwidth, efficient, electrically small antennas," *IEEE Antennas Wireless Propag. Lett.*, vol. 10, pp. 1582–1585, Jan. 5, 2012. doi: 10.1109/LAWP.2012.2182981.

[9] N. Zhu and R. W. Ziolkowski, "Broad-bandwidth, electrically small antenna augmented with an internal non-Foster element," *IEEE Antennas Wireless Propag. Lett.*, vol. 11, pp. 1116–1120, Sept. 2012. doi: 10.1109/LAWP.2012.2219572.

[10] C. R. White, J. S. Colburn, and R. G. Nagele, "A non-Foster VHF monopole antenna," *IEEE Antennas Wireless Propag. Lett.*, vol. 11, pp. 584–587, June 2012. doi: 10.1109/LAWP.2012.2201129.

[11] E. Ugarte-Munoz, S. Hrabar, D. Segovia-Vargas, and A. Kiricenko, "Stability of non-Foster reactive elements for use in active metamaterials and antennas," *IEEE Trans. Antennas Propag.*, vol. 60, no. 7, pp. 3490–3494, 2012. doi: 10.1109/TAP.2012.2196957.

[12] M. M. Jacob and D. F. Sievenpiper, "Gain and noise analysis of non-Foster matched antennas," *IEEE Trans. Antennas Propag.*, vol. 64, no. 12, pp. 4993–5004, 2016. doi: 10.1109/TAP.2016.2617380.

[13] S. Qin, Q. Xu, and Y. E. Wang, "Nonreciprocal components with distributedly modulated capacitors," *IEEE Trans. Microw. Theory Techn.*, vol. 62, no. 10, pp. 2260–2272, 2014. doi: 10.1109/TMTT.2014.2347935.

[14] P. Loghmannia and M. Manteghi, "Simultaneous Transmit and Receive (STAR): Circulators versus nonreciprocal antennas," in *Proc. IEEE Int. Symp. Antennas Propag. USNC-URSI Radio Sci. Meeting*, July 7–12, 2019, pp. 2171–2172. doi: 10.1109/APUSNCURSINRSM.2019.8888311.

[15] A. K. Kamal, "A parametric device as a nonreciprocal element," *Proc. IRE*, vol. 48, no. 8, pp. 1424–1430, 1960. doi: 10.1109/JRPROC.1960.287569.

[16] P. Loghmannia and M. Manteghi, "An active cavity-backed slot antenna based on a parametric amplifier," *IEEE Trans. Antennas Propag.*, vol. 67, no. 10, pp. 1–1, 2019. doi: 10.1109/TAP.2019.2920236.

[17] P. Loghmannia and M. Manteghi, "A parametric amplifier slot antenna," in *Proc. IEEE Int. Symp. Antennas Propag. USNC/URSI Nat. Radio Sci. Meeting*, July 8–13, 2018, pp. 487–488. doi: 10.1109/APUSNCURSINRSM.2018.8608664.

[18] H. Li, A. Mekawy, and A. Alù, "Beyond Chu's limit with Floquet impedance matching," *Phys. Rev. Lett.*, vol. 123, no. 16, p. 164102, 2019. doi: 10.1103/PhysRevLett.123.164102.

[19] R. E. Collin, "Parametric amplifiers," in *Found. Microw. Eng.: IEEE*, vol. 200, pp. 799–830.

[20] G. L. Matthaei, L. Young, and E. M. T. Jones, *Microwave Filters, Impedance-Matching Networks, and Coupling Structures*. Norwood, MA: Artech House, 1980.

[21] D. Natarajan, "A practical design of lumped, semi-lumped and microwave cavity filters," *Lecture Notes Elect. Eng.*, vol. 183, pp. 1–157, June 10, 2013. doi: 10.1007/978-3-642-32861-9_1.

[22] L. A. Blackwell and K. L. Kotzebue, *Semiconductor-Diode Parametric Amplifiers*. Englewood Cliff, NJ: Prentice Hall 1961.